Detection of magnetic fields in the circumgalactic medium of nearby galaxies using Faraday rotation

(article starts on next page)

Astronomy & Astrophysics

Detection of magnetic fields in the circumgalactic medium of nearby galaxies using Faraday rotation

V. Heesen[1], S. P. O'Sullivan[2], M. Brüggen[1], A. Basu[3], R. Beck[4], A. Seta[5], E. Carretti[6],
M. G. H. Krause[7], M. Haverkorn[8], S. Hutschenreuter[8], A. Bracco[9], M. Stein[10], D. J. Bomans[10],
R.-J. Dettmar[10], K. T. Chyży[11], G. H. Heald[12], R. Paladino[6], and C. Horellou[13]

[1] Hamburg University, Hamburger Sternwarte, Gojenbergsweg 112, 21029 Hamburg, Germany
   e-mail: volker.heesen@hs.uni-hamburg.de
[2] School of Physical Sciences and Centre for Astrophysics & Relativity, Dublin City University, Glasnevin D09 W6Y4, Ireland
[3] Thüringer Landessternwarte, Sternwarte 5, 07778 Tautenburg, Germany
[4] Max-Planck Institut für Radioastronomie, Auf dem Hügel 69, 53121 Bonn, Germany
[5] Research School of Astronomy and Astrophysics, Australian National University, Canberra, ACT 2611, Australia
[6] INAF, Istituto di Radioastronomia, Via Gobetti 101, 40129 Bologna, Italy
[7] Centre for Astrophysics Research, University of Hertfordshire, College Lane, Hatfield AL10 9AB, UK
[8] Department of Astrophysics/IMAPP, Radboud University, PO Box 9010, 6500 GL Nijmegen, The Netherlands
[9] Laboratoire de Physique École Normale Supérieure (LPENS), 24 rue Lhomond, 75005 Paris, France
[10] Ruhr University Bochum, Faculty of Physics and Astronomy, Astronomical Institute, 44780 Bochum, Germany
[11] Astronomical Observatory, Jagiellonian University, ul. Orla 171, 30-244 Kraków, Poland
[12] CSIRO Space and Astronomy, PO Box 1130, Bentley, WA 6102, Australia
[13] Dept of Space, Earth and Environment, Chalmers University of Technology, Onsala Space Observatory, 43992 Onsala, Sweden

ABSTRACT

Context. The existence of magnetic fields in the circumgalactic medium (CGM) is largely unconstrained. Their detection is important as magnetic fields can have a significant impact on the evolution of the CGM, and, in turn, the fields can serve as tracers for dynamical processes in the CGM.

Aims. Using the Faraday rotation of polarised background sources, we aim to detect a possible excess of the rotation measure in the surrounding area of nearby galaxies.

Methods. We used 2461 residual rotation measures (RRMs) observed with the LOw Frequency ARray (LOFAR), where the foreground contribution from the Milky Way is subtracted. The RRMs were then studied around a subset of 183 nearby galaxies that was selected by apparent B-band magnitude.

Results. We find that, in general, the RRMs show no significant excess for small impact parameters (i.e., the perpendicular distance to the line of sight). However, if we only consider galaxies at higher inclination angles and sightlines that pass close to the minor axis of the galaxies, we find significant excess at impact parameters of less than 100 kpc. The excess in |RRM| is 3.7 rad m^{-2} with an uncertainty between ±0.9 rad m^{-2} and ±1.3 rad m^{-2} depending on the statistical properties of the background (2.8σ–4.1σ). With electron densities of $\sim 10^{-4}$ cm^{-3}, this suggests magnetic field strengths of a few tenths of a microgauss.

Conclusions. Our results suggest a slow decrease in the magnetic field strength with distance from the galactic disc, as expected if the CGM is magnetised by galactic winds and outflows.

Key words. cosmic rays – galaxies: magnetic fields – galaxies: fundamental parameters – galaxies: ISM – radio continuum: galaxies

1. Introduction

The evolution of galaxies is regulated by the accretion and expulsion of matter that is related to feedback by either star formation or active galactic nuclei. In recent years it has become clear that galaxies are surrounded by large reservoirs of a diffuse, hot, and tenuous gas now referred to as the circumgalactic medium (CGM; Tumlinson et al. 2017; Faucher-Giguere & Oh 2023). While the CGM comprises multi-phase gas, it is so tenuous that it can be studied via absorption lines in the spectra of bright background quasars that show the presence of highly ionised species (Lehner et al. 2015; Werk et al. 2016); a tentative detection in X-ray emission was reported by Das et al. (2020). Theoretical work suggests that the CGM may have substantial pressure support from cosmic rays (Buck et al. 2020). Magnetic

fields are another pressure component that needs to be considered when determining the dynamics and structure of the CGM (van de Voort et al. 2021).

Two possible scenarios have been put forward to explain how the CGM might get magnetised: the magnetic fields are either generated in situ by turbulence via the small-scale dynamo (Pakmor et al. 2017) or they are transported from the galaxies via galactic winds (Péroux et al. 2020). Both models suggest that higher magnetic field strengths are found near the minor axis of galaxies as outflows, either stellar- (Thomas et al. 2022) or active-galactic-nucleus-driven (Pillepich et al. 2021), and are driven most easily along the minor axis, which both transports magnetic fields and generates turbulence. The processes that magnetise the CGM will also influence its structure. The small-scale dynamo preferentially generates turbulent

magnetic fields; via shear, these magnetic fields can be converted into anisotropic fields (Fletcher et al. 2011). If shear exists in the CGM on sufficiently large scales, one can expect anisotropic random fields on scales of tens of kiloparsecs. Similarly, if the gaseous halo of a galaxy hosts a dynamo, one would have large-scale magnetic field configurations (Moss et al. 2010). Lastly, models of galactic winds show a helical magnetic field structure that results in a large-scale ordering (Zirakashvili et al. 1996; Henriksen & Irwin 2016; Thomas et al. 2022); such large-scale helical magnetic fields have indeed been found in galaxy haloes (Mora-Partiarroyo et al. 2019; Stein et al. 2020).

Because magnetic fields in the CGM are expected to be weak, they can be detected best via the Faraday rotation of polarised background sources, rather than directly via synchrotron emission due to the effects of spectral ageing (Miskolczi et al. 2019). Faraday rotation can be described by a wavelength-dependent shift in the polarisation angle,

$$\varphi(\lambda) = \varphi_0 + \text{RM}\lambda^2, \tag{1}$$

where φ and φ_0 are the observed and intrinsic polarisation angles, respectively, RM is the rotation measure, and λ is the wavelength. This definition of the RM is only valid for a synchrotron source behind the Faraday rotating medium, whereas mixed media are described by a Faraday spectrum with various Faraday rotating components, called Faraday complexity (Brentjens & de Bruyn 2005). Neglecting Faraday complexity, the RM is the line-of-sight (LoS) integral,

$$\text{RM} = 0.81 \int_{\text{LoS}} \left(\frac{n_e}{\text{cm}^{-3}}\right)\left(\frac{B_\parallel}{\mu\text{G}}\right)\left(\frac{\text{d}r}{\text{pc}}\right) \text{rad m}^{-2}, \tag{2}$$

where n_e is the electron number density and $B_\parallel$ the strength of the magnetic field component along the LoS. One way to study the effect of the CGM is to use background sources where a Mg II quasar absorption line is detected, which is indicative of the presence of ionised gas (Kacprzak et al. 2008). It has been shown that Mg II absorbers have higher absolute RM values, |RM|, than the control sample at frequencies of 5 GHz (Bernet et al. 2008, 2010) but possibly not at lower frequencies (Bernet et al. 2012). At lower frequencies, the effect of Faraday rotation becomes stronger (see Eq. (1)), so an inhomogeneous distribution of the RM can lead to increased depolarisation (Kim et al. 2016). However, at 1.4 GHz, Farnes et al. (2014) were able to show that, even at such a low frequency, the excess in |RM| can still be seen. Farnes et al. (2014) also find that the excess is only found in sources where the sightlines to the quasar and the polarised emission are in good agreement. More recently, however, these results have been questioned by Lan & Prochaska (2020) and Amaral et al. (2021), who do not find a correlation of |RM| with the number of foreground galaxies; much larger and precise datasets are required to study this further (Basu et al. 2018; Shah & Seta 2021).

Studies thus far have concentrated on galaxies at moderate redshifts ($z \sim 0.5$) as they are more prone to show strong absorption lines. However, this has a downside because the measurable RM signal is suppressed by a factor of $(1 + z)^{-2}$. It is, however, an intriguing possibility that ordinary nearby galaxies are also surrounded by a magnetised CGM that can potentially be detected with this method. This has now become feasible as low-frequency radio continuum polarimetry leads to a higher precision, such as by using the LOw Frequency ARray (LOFAR; van Haarlem et al. 2013). Using data from the LOFAR Two-metre Sky Survey (LoTSS; Shimwell et al. 2017, 2019), O'Sullivan et al. (2023) find 2461 polarised sources at 144 MHz.

Compared with current surveys at 1.4 GHz, the source density per sky area is about five times lower due to depolarisation, but the values of the RM can be much more precise because of the strong wavelength dependence. In this Letter we probe the excess |RM| as a function of the impact parameter of nearby galaxies with an apparent optical B-band magnitude of $m_B < 12.5$ mag drawn from the Palomar sample of Ho et al. (1997). We find a marginally significant ($\gtrsim 2\sigma$) excess of |RM| at impact parameters less than 100 kpc, which indicates the presence of a magnetised CGM.

2. Data and methodology

We used a catalogue of high-precision Faraday RMs from O'Sullivan et al. (2023), who present 2461 extragalactic sources. These RMs have a median uncertainty of only 0.06 rad m^{-2}, which is the random uncertainty, although a higher systematic error of 0.3 rad m^{-2} is possible after ionospheric correction. Comparisons with centimetre-wavelength RMs indicate minimal amounts of Faraday complexity (Livingston et al. 2021) in the LoTSS detections, meaning that they are well suited for studying Faraday rotation in the foreground. These data were taken at a frequency of 144 MHz and at an angular resolution of 20″ using the LOFAR High-Band Antennas (van Haarlem et al. 2013). The sources are distributed over an area of 5720 deg^2 on the sky using data from the LoTSS Data Release 2 (LoTSS-DR2; Shimwell et al. 2022) observed at declinations greater than 0° with a frequency range between 120 and 168 MHz. The Milky Way contribution to the RM, the Galactic rotation measure (GRM), is subtracted, leaving us with the residual rotation measure (RRM): RRM = RM − GRM, using the GRM model from Hutschenreuter & Enßlin (2020). In particular, we used the mean value of the reconstructed Faraday sky (i.e., the GRM) constrained by RM values with a typical separation of 1° (Oppermann et al. 2012) and also constrained by the emission measure data from *Planck* (Planck Collaboration X 2016). The LoTSS RM values are not included in this GRM reconstruction. We subtracted the GRM from the LoTSS RM at the location of each source using the interpolated value of the four nearest neighbours in the GRM map. We also tested averaging the GRM value over a disc of 1° in diameter as well as using the GRM map, which is not constrained by the emission measure data. In both cases, this had an insignificant effect on the results.

We selected galaxies from the Palomar sample of Ho et al. (1997), 183 of which overlapped with our covered area. This sample is magnitude selected, so it contains the brightest nearby galaxies where our subset has a median distance of 18 Mpc (3.2–109 Mpc). We obtained coordinates in right ascension (α) and declination (δ) from the NASA Extragalactic Database (NED). We also obtained redshift-independent measurements of the distance to the galaxies from NED, giving preference to distances obtained with Cepheids or the method using the tip of the red giant branch. If that was not available, we used distances from the Tully–Fisher relation or the method of brightest stars. We obtained the positions and inclination angles from the Hyper-LEDA data base (Makarov et al. 2014). We used 2 μm fluxes from the Two Micron All Sky Survey (Huchra et al. 2012) to calculate stellar masses.

For each polarised background source, we then calculated the impact parameters as the perpendicular distance between the LoS and the galaxies via

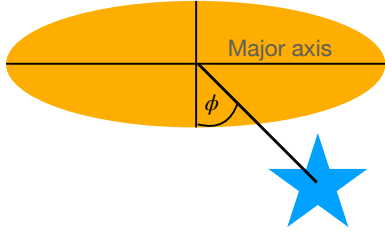$$b_{jk} = 17.5 \sqrt{\cos^2(\delta_k)(\alpha_j - \alpha_k)^2 + (\delta_j - \delta_k)^2} d_k \text{ kpc}, \tag{3}$$

Fig. 1. Azimuthal angle, ϕ, of the polarised background source with respect to the minor axis. Sources near the minor axis have $|\phi| < 45°$, whereas sources near the major axis have $|\phi| > 45°$.

where j specifies the background source and k the foreground galaxy. The units for $\alpha_{j,k}$ and $\delta_{j,k}$ are degrees and the distance, d_k, is in units of Mpc. The minimum impact parameter, b, for each background source was then retained. We also calculated the azimuthal angle for each background source with respect to the minor axis of the galaxy, where an azimuthal angle of 0° means that the source is lying along the minor axis of the galaxy (see Fig. 1). Any galaxies from the Local Group at $d < 1$ Mpc were excluded as their signal, having an apparent scale of several degrees, would be subtracted together with the Milky Way foreground.

3. Results

First, we analysed the RRM for all galaxies, finding no excess of |RRM| at small impact parameters (not shown here). Next, we analysed the RRM for all inclined galaxies (i.e., with an inclination angle $i \geq 55°$). If we select only galaxies where the background source lies near the minor axis with $|\phi| < 45°$, as shown in Fig. 2 (left panel), we find an excess of |RRM| for impact parameters $b < 100$ kpc, where the median |RRM| is 7.8 ± 0.9 rad m^{-2}; we estimated the error by bootstrapping. For impact parameters $100 < b/\mathrm{kpc} < 1000$, the distribution of the binned median in 100 kpc intervals, |RRM|, is nearly flat and can be fitted with a constant value of 4.1 ± 0.2 rad m^{-2}. Hence, the |RRM| excess would be 3.7 ± 0.9 rad m^{-2} at a 4.1σ significance. This assumes that all sightlines at $b > 100$ kpc trace the background and contain no signal. A more conservative estimate of the background uncertainty is to calculate the running median with a binning size of 29 data points, which is the number of sightlines at $b < 100$ kpc. The standard deviation of these median |RRM| values is 1.0 rad m^{-2}, which means our background |RRM| estimate is 4.1 ± 1.0 rad m^{-2}. Thus, the excess |RRM| at small impact parameters is 3.7 ± 1.3 rad m^{-2}, equating to a 2.8σ significance.

The fact that the sightlines with $b < 100$ kpc show an excess of |RRM| can also be seen in the cumulative distribution function shown in Fig. 2 (right panel). A two-sample Kolmogorov–Smirnov test shows that the distribution of the |RRM| for $b < 100$ kpc has less than a 3% probability of agreeing with any of the other 100 kpc bins, with an average probability of 0.5%. Also, we note that the median photometric redshift for sources at $b < 100$ kpc, $z = 0.56 \pm 0.41$, is smaller than for sources at $b > 100$ kpc, for which it is 0.69 ± 0.43. Hence, the |RRM| excess cannot be explained by the boosting of the intrinsic source RM with higher redshift as the effect is less than 10% (Basu et al. 2018). There is no difference between group and non-group members (Garcia 1993). A similar trend of |RRM| with the impact parameter is also seen from analytical models of thermal electron density and magnetic fields (see Fig. 10 in Shah & Seta

2021). The standard deviation for the |RRM| of all sightlines is 5.5 rad m^{-2}. Both values are in good agreement with the upper limit of ≈ 6 rad m^{-2} for the extragalactic contribution (Schnitzeler 2010; Vacca et al. 2016), suggesting that the origin of the scatter is the intrinsic RMs of the sources and the contribution from cosmic web filaments (Carretti et al. 2023), and a possible contribution from the Galactic foreground on scales of less than 1° (Sun & Reich 2009).

If we select galaxies where the background source lies near the major axis with $|\phi| > 45°$, the excess |RRM| vanishes. This can be seen in Fig. 3, where we show the |RRM| dependence on the azimuthal angle relative to the disc minor axis. Values of |RRM| near the minor axis show an excess at small impact parameters in comparison with sources near the major axis. The difference disappears at larger impact parameters because the polar quadrants ($|\phi| < 45°$) have a much steeper radial decline in |RRM|. By comparison, the radial profile in the plane of the disc is rather flat and agrees with the polar one at $b > 200$ kpc. A similar effect is presented in Fig. 4, which shows the azimuthal dependence for three radial bins of impact parameters. At small impact parameters, there is an azimuthal gradient in |RRM| from the poles down to the plane of the disc, with an |RRM| about two times higher. This could be taken as evidence that the |RRM| excess at low impact parameters $\lesssim 100$ kpc originates from the bipolar regions aligned with the minor axes of the galaxies. The dependence on the azimuthal angle has been observed in quasi-stellar-object absorption line measurements of Mg II (Bouché et al. 2012), where a bimodal distribution along the major and minor axis points to either large gaseous discs or galactic winds. Similarly, Bordoloi et al. (2011) find that only inclined galaxies ($i > 50°$) show an excess of Mg II absorption along the minor axis.

4. Discussion

For the first time, our data show that an excess of |RRM| along sightlines around nearby galaxies can be detected along the minor axis of inclined galaxies for impact parameters of less than 100 kpc. The dependence on azimuthal angle is in agreement with quasi-stellar-object absorption line measurements that trace the presence of ionised gas. Also, the median mass of our galaxies with sightlines $b < 100$ kpc is $M_\star = 10^{9.1 \pm 0.9}\,M_\odot$. Simulations show that biconical winds form in such galaxies with total masses between 10^{10} and $10^{11}\,M_\odot$ (assuming a 10% baryonic to total mass ratio); for lower masses the winds are spherical, whereas for higher masses they do not reach beyond the virial radius (≥ 150 kpc; Jacob et al. 2018). Hence, we argue that this effect is real and that the excess can be attributed to the CGM of the observed galaxies. The observed excess of 3.7 ± 1.3 rad m^{-2} is much smaller than the 24 ± 6 rad m^{-2} reported by Farnes et al. (2014) in Mg II absorbers and even smaller than the ≈ 140 rad m^{-2} of Bernet et al. (2008). This is certainly an effect of the insensitivity to large |RM| values, $\gtrsim 50$ rad m^{-2}, at LOFAR frequencies (Heald et al. 2009).

With an assumption of electron density, n_e, we can thus calculate the strength of the LoS component of the ordered magnetic field, $B_\parallel$, from Eq. (2). The current best estimate of the electron density in the CGM of the Milky Way is $\approx 10^{-4}$ cm^{-3} at radii ≈ 50–100 kpc (see Fig. 10 in Donahue & Voit 2022). With a LoS length of 100 kpc, we obtain an average strength of the LoS magnetic field of $\approx 0.5\,\mu$G. The energy density of this field component is $U_B \approx 10^{-14}$ erg cm^{-3}, in good agreement with the thermal energy density of the hot CGM ($T \approx 10^6$ K), meaning that we find a plasma beta of $\beta \approx 1$. We note that this is an upper
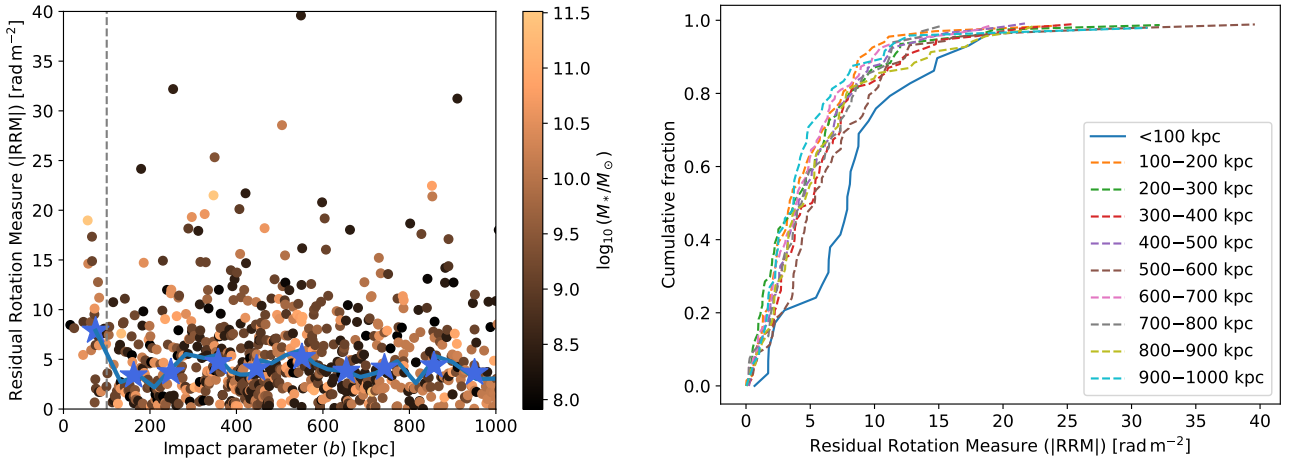
Fig. 2. Excess |RRM| at small impact parameters to the foreground galaxies. *Left panel*: |RRM| as a function of impact parameter for inclined galaxies ($i \geq 55°$) where the background polarised source lies near the minor axis ($|\phi| < 45°$). Data points are coloured according to the stellar mass of the foreground galaxy. Blue stars show the median |RRM| binned in 100 kpc intervals; the standard deviation is 0.57 ± 0.13 rad m^{-2} ($b > 100$ kpc) and 1.1 rad m^{-2} ($b < 100$ kpc). The solid blue line shows the running median of 29 binned data points, and the vertical dashed line is at $b = 100$ kpc. *Right panel*: cumulative distribution function of the |RRM| for sightlines binned into 100 kpc intervals. The solid blue line shows sightlines with $b < 100$ kpc, whereas the dashed coloured lines show them for $b > 100$ kpc.
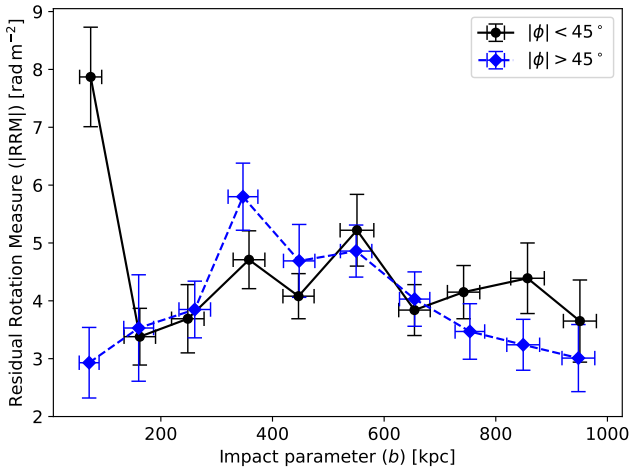
Fig. 3. |RRM| as a function of the impact parameter for different azimuthal angles relative to the disc minor axis for inclined galaxies. The filled black circles with solid lines are the measured |RRM| values close to the minor axis of the disc (i.e., $|\phi| < 45°$), and the dashed line with filled diamonds give the measured |RRM| values near the major axis of the disc (i.e., $|\phi| > 45°$). The error bars of the impact parameter give the standard deviation and those of |RRM| the standard error of the mean.
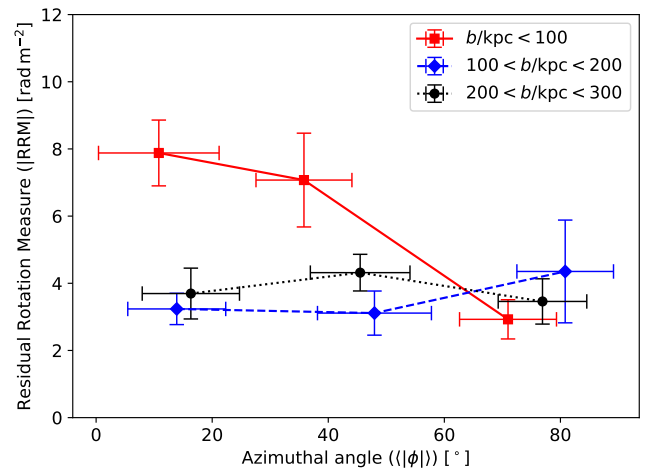
Fig. 4. Dependence of the |RRM| on the azimuthal angle relative to the disc minor axis for inclined galaxies. Three azimuthal angular bins within $0° < |\phi| < 30°$, $30° < |\phi| < 60°$, and $60 < |\phi| < 90°$ of the minor axis are defined for each of the three bins in terms of the impact parameter: $b < 100$ kpc (red squares), 100 kpc $< b < 200$ kpc (blue diamonds), and 200 kpc $< b < 300$ kpc (black circles). The error bars of the angles are the standard deviation of the mean of the azimuthal angles within that bin.

limit because the magnetic field strength may be higher since magnetic field reversals can lower the RM. Assuming a random distribution of the magnetic field with a coherence length of $l_c \approx 30$ kpc (as in the intra-cluster medium; Subramanian et al. 2006), the actual field strength would be a factor of $\sqrt{L/l_c} \approx 2$ higher. We note that the contribution from turbulent fields in the CGM on scales smaller than the projected size of the background polarised emission can also, in part, contribute to an excess of |RRM| (Basu et al. 2018). We have ignored such contributions as this would require additional information on the nature of the frequency-dependent Faraday depolarisation. Using data from the Very Large Array Sky Survey (Condon et al. 1998), Nilsson (2016) find a decrease in the amount of polarised sources near

galaxies and interpreted this as evidence for depolarisation by galactic halos.

The magnetic field strength in the CGM is about one-tenth of the strength of the ordered magnetic field in the discs of galaxies, which points to a rather slow decrease with distance, r, from the galactic disc. Observations of nearby galaxies show for the total magnetic field $B = B_0 \exp(-r/r_0)$, where $B_0 \approx 10$ μG and $r_0 \approx 10$ kpc (Beck 2015). For the ordered field, significantly higher scale heights are found (Krause et al. 2020). Assuming $r_0 \approx 20$ kpc and $B_0 \approx 5$ μG, the ordered field strength would be the correct strength at $r = 50$ kpc. Such high magnetic field strengths are indeed seen in simulations (Pakmor et al. 2020; Thomas et al. 2022). One can also explain the higher polar RRM with a specific chimney structure, such as seen in simulations,

where one would expect $\beta \approx 1$ from the shear between chimneys and halo gas (Rodgers-Lee et al. 2019; Krause et al. 2021).

5. Conclusions

We used observations of the RM of linearly polarised background sources with LOFAR to detect the magnetic field in the CGM surrounding nearby galaxies. We chose the apparent luminosity-selected Palomar catalogue of nearby galaxies and the RM catalogue from O'Sullivan et al. (2023). We subtracted the foreground RM from the Milky Way to obtain the RRM. Below we summarise our conclusions:

1. If we consider only inclined galaxies (inclination angle larger than 55°) and background sources within 45° of the minor axis, we find a moderate excess of |RRM| at impact parameters of <100 kpc of 3.7 rad m^{-2} with an uncertainty between 0.9 and 1.3 rad m^{-2} (2.8σ–4.1σ).
2. In contrast, no |RRM| excess is found for background sources within 45° of the major axis.
3. The dependence on azimuthal angle is limited to impact parameters smaller than 100 kpc, showing the maximum extent of the magnetised CGM detectable with this method and instrument.
4. For an order-of-magnitude estimate, we assume an electron density of 10^{-4} cm^{-3} and a sightline length of 100 kpc, which provides us with an average strength of the LoS magnetic field of 0.5 μG.

Our new results are in agreement with upper limits on |RRM| in the CGM in previous observations (Lan & Prochaska 2020) and suggest that magnetised bipolar galactic winds exist. Thus far, our method exploits only statistical properties of galaxies because for studies of individual galaxies the source density is too low. In the future, with more sensitive low-frequency telescopes, such as the upgraded LOFAR2.0 and the Square Kilometre Array, individual galaxies may come within reach, allowing the magnetic field structure to be studied in detail. For instance, the opening angle of the outflow cone or a change of the sign of the RRM across either major or minor axes, which would provide hints to the large-scale field structure, could be investigated. A complementary approach is to use high-frequency data such as from MeerKAT and the Australian Square Kilometre Array Pathfinder.

References

Amaral, A. D., Vernstrom, T., & Gaensler, B. M. 2021, MNRAS, 503, 2913
Basu, A., Mao, S. A., Fletcher, A., et al. 2018, MNRAS, 477, 2528
Beck, R. 2015, A&ARv, 24, 4
Bernet, M. L., Miniati, F., Lilly, S. J., Kronberg, P. P., & Dessauges-Zavadsky, M. 2008, Nature, 454, 302
Bernet, M. L., Miniati, F., & Lilly, S. J. 2010, ApJ, 711, 380
Bernet, M. L., Miniati, F., & Lilly, S. J. 2012, ApJ, 761, 144
Bordoloi, R., Lilly, S. J., Knobel, C., et al. 2011, ApJ, 743, 10
Bouché, N., Hohensee, W., Vargas, R., et al. 2012, MNRAS, 426, 801
Brentjens, M. A., & de Bruyn, A. G. 2005, A&A, 441, 1217
Buck, T., Pfrommer, C., Pakmor, R., Grand, R. J. J., & Springel, V. 2020, MNRAS, 497, 1712
Carretti, E., O'Sullivan, S. P., Vacca, V., et al. 2023, MNRAS, 518, 2273
Condon, J. J., Cotton, W. D., Greisen, E. W., et al. 1998, AJ, 115, 1693
Das, S., Mathur, S., & Gupta, A. 2020, ApJ, 897, 63
Donahue, M., & Voit, G. M. 2022, Phys. Rep., 973, 1
Farnes, J. S., O'Sullivan, S. P., Corrigan, M. E., & Gaensler, B. M. 2014, ApJ, 795, 63
Faucher-Giguere, C. A., & Oh, S. P. 2023, ARA&A, submitted [arXiv:2301.10253]
Fletcher, A., Beck, R., Shukurov, A., Berkhuijsen, E. M., & Horellou, C. 2011, MNRAS, 412, 2396
Garcia, A. M. 1993, A&AS, 100, 47
Heald, G., Braun, R., & Edmonds, R. 2009, A&A, 503, 409
Henriksen, R. N., & Irwin, J. A. 2016, MNRAS, 458, 4210
Ho, L. C., Filippenko, A. V., & Sargent, W. L. W. 1997, ApJS, 112, 315
Huchra, J. P., Macri, L. M., Masters, K. L., et al. 2012, ApJS, 199, 26
Hutschenreuter, S., & Enßlin, T. A. 2020, A&A, 633, A150
Jacob, S., Pakmor, R., Simpson, C. M., Springel, V., & Pfrommer, C. 2018, MNRAS, 475, 570
Kacprzak, G. G., Churchill, C. W., Steidel, C. C., & Murphy, M. T. 2008, AJ, 135, 922
Kim, K. S., Lilly, S. J., Miniati, F., et al. 2016, ApJ, 829, 133
Krause, M., Irwin, J., Schmidt, P., et al. 2020, A&A, 639, A112
Krause, M. G. H., Rodgers-Lee, D., Dale, J. E., Diehl, R., & Kobayashi, C. 2021, MNRAS, 501, 210
Lan, T.-W., & Prochaska, J. X. 2020, MNRAS, 496, 3142
Lehner, N., Howk, J. C., & Wakker, B. P. 2015, ApJ, 804, 79
Livingston, J. D., McClure-Griffiths, N. M., Gaensler, B. M., Seta, A., & Alger, M. J. 2021, MNRAS, 502, 3814
Makarov, D., Prugniel, P., Terekhova, N., Courtois, H., & Vauglin, I. 2014, A&A, 570, A13
Miskolczi, A., Heesen, V., Horellou, C., et al. 2019, A&A, 622, A9
Mora-Partiarroyo, S. C., Krause, M., Basu, A., et al. 2019, A&A, 632, A11
Moss, D., Sokoloff, D., Beck, R., & Krause, M. 2010, A&A, 512, A61
Nilsson, N. 2016, Master's thesis (Gothenburg, Sweden: Chalmers University of Technology)
Oppermann, N., Junklewitz, H., Robbers, G., et al. 2012, A&A, 542, A93
O'Sullivan, S. P., Shimwell, T. W., Hardcastle, M. J., et al. 2023, MNRAS
Pakmor, R., Gómez, F. A., Grand, R. J. J., et al. 2017, MNRAS, 469, 3185
Pakmor, R., van de Voort, F., Bieri, R., et al. 2020, MNRAS, 498, 3125
Péroux, C., Nelson, D., van de Voort, F., et al. 2020, MNRAS, 499, 2462
Pillepich, A., Nelson, D., Truong, N., et al. 2021, MNRAS, 508, 4667
Planck Collaboration X 2016, A&A, 594, A10
Rodgers-Lee, D., Krause, M. G. H., Dale, J., & Diehl, R. 2019, MNRAS, 490, 1894
Schnitzeler, D. H. F. M. 2010, MNRAS, 409, L99
Shah, H., & Seta, A. 2021, MNRAS, 508, 1371
Shimwell, T. W., Röttgering, H. J. A., Best, P. N., et al. 2017, A&A, 598, A104
Shimwell, T. W., Tasse, C., Hardcastle, M. J., et al. 2019, A&A, 622, A1
Shimwell, T. W., Hardcastle, M. J., Tasse, C., et al. 2022, A&A, 659, A1
Stein, Y., Dettmar, R. J., Beck, R., et al. 2020, A&A, 639, A111
Subramanian, K., Shukurov, A., & Haugen, N. E. L. 2006, MNRAS, 366, 1437
Sun, X. H., & Reich, W. 2009, A&A, 507, 1087
Thomas, T., Pfrommer, C., & Pakmor, R. 2022, MNRAS, submitted [arXiv:2203.12029]
Tumlinson, J., Peeples, M. S., & Werk, J. K. 2017, ARA&A, 55, 389
Vacca, V., Oppermann, N., Enßlin, T., et al. 2016, A&A, 591, A13
van de Voort, F., Bieri, R., Pakmor, R., et al. 2021, MNRAS, 501, 4888
van Haarlem, M. P., Wise, M. W., Gunst, A. W., et al. 2013, A&A, 556, A2
Werk, J. K., Prochaska, J. X., Cantalupo, S., et al. 2016, ApJ, 833, 54
Zirakashvili, V. N., Breitschwerdt, D., Ptuskin, V. S., & Völk, H. J. 1996, A&A, 311, 113